DIGITAL IMAGE ANALYSIS OF DISTRIBUTION OF IMMISCIBLE FLUIDS IN NATURAL POROUS MEDIA

Marcos A. Montoro[(1)] and Franco M. Francisca[(2)]

ABSTRACT

This article proposes a method of digital image analysis to monitor immiscible displacement in soil samples. Four different natural soil samples were studied: coarse, medium, fine and silty sand. Paraffin oil and a sodium fluorescein solution were used as the displaced and displacing phase, respectively. Immiscible displacement tests were performed in a plexiglass cell and monitored by means of digital image analysis and direct volumetric measurement. The images were processed to obtain gray levels at different stages during the tests. Saturation of paraffin oil was then computed from the gray level and a linear regression equation was developed for each soil tested. The proposed method enabled valuable information to be obtained of the processes that take place at the face of the samples during displacement and in the middle of the samples at the end of the tests. This procedure was very effective for analyzing different flow patterns, isolating areas with trapped paraffin oil, and to determining the ganglia size distribution at different stages of the immiscible displacement tests. The results indicated that particle size and microstructure heterogeneities determine the flow pattern features observed during the immiscible displacement of paraffin oil by water.

KEYWORDS: Immiscible displacement; LNAPL; digital image analysis; remediation.

[1]Postdoctoral fellow, CONICET and Adjunct Professor, Universidad Nacional de Córdoba, Córdoba, Argentina.

[2] Adjunct Researcher, CONICET and Adjunct Professor, Universidad Nacional de Córdoba, Córdoba, Argentina.
Departamento de Construcciones Civiles
Av. Velez Sarsfield 1611, 5016, Córdoba, Argentina
E-mail: ffrancis@efn.uncor.edu
(Corresponding author)

INTRODUCTION

There are different situations that involve immiscible displacement of fluids in natural porous media, including the simultaneous flow of oil and water during oil recovery in reservoirs (Donaldson *et al.* 1985), the migration of Non-Aqueous Phase Liquids (NAPL) in soils and rocks due to accidental spills, and during the remediation of a NAPL contaminated site. These situations have economic and environmental impact (Babadagli 2007; Suthersan 1997).

There are many different NAPLs, with a wide variety of physical and chemical properties. Depending on the relative density of the NAPL, it can be classified as lighter than water (LNAPL) or denser than water (DNAPL). When a NAPL is spilled on the soil, it may displace air or water from soil pores, depending on the fluid density, water table position and the hydrogeology of the site.

A fraction of NAPL remains trapped inside the soil pores, forming ganglia during the immiscible displacement under either drainage or imbibition conditions. Immiscible flow and ganglia formation/mobilization are governed by gravity and viscous and capillary forces (Mercer and Cohen 1990). Gravity forces appear because of the density difference between fluid phases, capillary forces result from the presence of interfaces, and viscous forces from the effect of the relative displacement between both fluids (Pennell *et al.* 1996).

The spatial distribution of immiscible fluids in soil depends on many properties of soils and fluids. The most important of these are soil porosity, pore sizes and pore size distribution, grain wettability, volumetric content of each fluid phase, fluid viscosity, density and interfacial tension (Mercer and Cohen 1990; Newell *et al.* 1995).

Ganglia generation and mobilization are not usually considered in traditional analytical formulations. Soils are frequently considered as equivalent continuous media, where the relative saturation of each phase and relative hydraulic conductivity are used to understand immiscible displacement in soil pores. However, soils and rocks are not homogeneous, and the entrapment and mobilization of ganglia can only be observed by means of micro-scale analysis (Sahimi 1993; Wildenschild *et al*. 2005). This phenomenon is of fundamental importance, given that it controls residual saturation and the efficiency of remediation processes (Sharma and Reddy 2004). Numerical methods such as pore networks and cellular automata are very useful tools to

study the behavior of immiscible liquids inside porous media, but this type of formulation usually requires great computational efforts (Chen *et al.* 2006).

Physical processes involving ganglia formation/mobilization can also be studied by means of laboratory tests, which are usually monitored by means of an imaging technique. The most common imaging techniques applied in geotechnical engineering and in hydrogeology include light transmission or light reflection methods, X-ray microtomography, gamma radiation or nuclear magnetic resonance imaging. Digital image analysis acquired from light transmission and light reflection techniques are among the most commonly used methods for fluid displacement characterization, since the other techniques require relatively complex devices and data acquisition systems (Werth *et al.* 2010). The main restriction for most of these techniques is that either extremely small samples or synthetic materials should be used to evaluate physical processes that take place at pore level (Lenormand *et al.* 1988; Silin *et al.* 2011).

Glass beads and manufactured glass sheets with carefully designed pore bodies and pore throat sizes and distribution are the most common synthetic materials employed to perform immiscible fluid flow tests, monitored by either light transmission or light reflection methods (Jia *et al.* 1999; Tsakiroglou *et al.* 2003). Commonly employed synthetic grain sizes range between 50 and 2000 μm (Al-Raoush and Wilson 2005; Oostrom *et al*. 2007; Aggelopoulos and Tsakiroglou 2009), but these sizes are far from reproducing clay and silt particles sizes.

More recently, there has been considerable effort to find synthetic transparent soils to improve light imaging techniques. The materials studied include silica gel, fused silica, fumed silica and Aquabeads (Peters *et al*. 2011; Lo *et al.* 2010; Zhao *et al.* 2010). The principle applied to obtain a transparent translucent soil is to match the refractive index of the solid material and the fluid phase (Peters *et al.* 2011). Usually it is necessary to use a combination of fluids, some of which are harmful and complicated to handle (Lo *et al.* 2010). These materials have been geotechnically characterized and most of them have macro-mechanical and hydraulic properties that make it possible to simulate soils from sands to clays (Iskander *et al.* 2002; Ezzein and Bathurst 2011).

However there are many problems with using this kind of materials to study contaminant transport through soils. For instance, Aquabeads are a soft water-based polymer that can undergo significant volume changes resulting from small increases in the confining pressure, which limits

the application of these materials for flexible wall permeameter tests (Lo *et al.* 2010). But the most important considerations are related to the fluids that are required to achieve transparent soils. Zhao *et al.* (2010) investigated twelve different fluids in order to obtain transparent soils and determined that mixtures of toluene and methyl ethyl ketone and toluene – 2 propanol show a good refractive index, with a viscosity similar to water. This is an important problem because it limits the type of contaminants transport that can be simulated with these materials. The need for a fluid with a particular refraction index does not guarantee proper ratios between the interfacial tensions among the different phases that determine the magnitude of capillary forces and ganglia formation/displacement during immiscible flow phenomena.

In addition, the main problem of these tests is that, in general, they fail to reproduce important particle-fluid interactions that may control the displacement of liquids in natural porous media (Montoro and Francisca 2010).

It is important to note that there is no published attempt to apply light reflection methods to the study of immiscible displacement in natural porous media or to determine and study the ganglia sizes and size distributions.

Other alternatives for imaging natural porous media include the use of X-ray microtomography, gamma radiation or nuclear magnetic resonance imaging. Goldstein *et al*. (2007) successfully imaged natural porous media with a significant content of clay and silt particles, after injecting a known amount of gasoline in a medical magnetic resonance imaging device. The main problems of this technique are the complexity of the devices and data processing required and the impossibility of monitoring the process, since the tomography can only be made for the final state or flow process interruptions are required at intermediate stages.

The objective of this research is to extend the application of light reflection methods for the study of natural soil samples by developing accurate correlations between the light intensity reflected by soil samples and the amount of NAPL inside soil pores. The main purpose is to evaluate the evolution of immiscible displacement patterns and ganglia sizes at different stages during NAPL imbibition.

BACKGROUND

Immiscible flow

The simultaneous immiscible flow of two different fluid phases is described by means of the mass conservation equation (Equation 1) and the generalized Darcy's law (Equation 2) (Chen *et al.* 2006; Dullien 1992):

$$\frac{\partial(n\rho_N S_N)}{\partial t} = -\nabla \cdot (\rho_N v_N) + s_N \tag{1}$$

$$v_N = -\frac{1}{\mu_N} k_{rN} K(\nabla P_N - \rho_N g \nabla x) \tag{2}$$

where n is soil porosity, ρ is fluid density, t is time, S is fluid saturation, v is flow velocity and s are sink and sources within the considered domain, sub index N represents each fluid phase present in the media, μ is fluid viscosity, K is the intrinsic permeability of the porous media, k_{rN} is the relative permeability, P is the hydraulic pressure, g is the acceleration of the gravity field and x is the position.

To solve equations (1) and (2) it is most important to know how capillary pressure and relative permeability change with the degree of saturation of each fluid phase during the displacement process (Dullien 1992). Panfilov and Panfilova (2005) suggested a modification of the macroscopic constitutive formulation (Equations 1 and 2); incorporating emergent behaviors obtained from pore networks simulations. Recently, van Duijn *et al.* (2007) proposed a Buckley–Leverett-like solution, considering NAPL trapping in a heterogeneous porous media. This solution enabled preferential ganglia formation to be predicted at the interfaces between materials of different pore sizes.

The only successful analytical way to consider the pore scale processes involved during immiscible displacement of NAPL by water is by means of pore networks simulations (Blunt 2001). This modeling technique was effectively employed to study different aspects of immiscible displacement phenomena, the most important of which are the application of pore networks to determine the effect of the correlation length and spatial variability of pore sizes on ganglia size and distribution (Francisca and Arduino 2007), the quantification of dynamic effects on capillary pressure changes (Hassanizadeh and Gray 1993), the study of relative permeability (Karaman and Demiral 2004), the assessment of relative permeability hysteresis for drainage–imbibition processes (Ahrenholz *et al.* 2008), and the effect of NAPL dissolution during flow (Dillard and Blunt 2000). However, the problem with this powerful numerical tool is that it still

demands significant computational efforts when analyzing porous media of medium complexity (Blunt 2001). It is also extremely difficult to obtain the representative pore-scale soil properties needed to develop reliable pore networks models. This shows that laboratory methods and experimental researches are of great importance for the study of these phenomena (Al-Raoush and Willson 2005).

Digital image analysis

There are many different imaging techniques suitable for studying porous media, including light transmission methods, light reflection methods, gamma radiation, X-ray microtomography and magnetic resonance imaging. Each method has advantages and disadvantages for obtaining different porous media properties. Werth *et al*. (2010) presented a detailed review of the main features and applications of these techniques, selecting the light reflection-based method due to its low cost, fast acquisition time and simplicity of operation. No matter which method is employed, the data obtained can be summarized as a digital image.

Digital images can be considered as a matrix in which each pixel $I_{(x,y)}$ is described by a vector of three components, with x and y giving the position of the pixel in the matrix. Each component of the vector represents something different, according to the system selected to represent the image. The red, green, blue system (RGB) or hue, saturation and value (HSV) are the most common systems for representing images.

Color images can be transformed into a gray scale image by means of simple arithmetic operations. In gray scale images, each pixel is represented by a single numerical value instead of a vector. That number is known as a gray level or digital level (GL) and for 8-bits images it runs from 0 (black) to 255 (white).

Digital images acquired by light reflection methods or light transmission methods were initially employed to determine moisture content (Darnault *et al*. 1998), qualitatively monitor the dispersion and concentration of contaminant in porous media, and evaluate contaminant concentration and distribution (Dong and Selvadurai 2006), as well as to evaluate fingering characteristics during DNAPL displacement (Smith and Zang 2001, Zang and Smith 2001).

Light transmission methods are based on light absorption, diffraction and transmission through a translucent media. These methods have the inconvenience that they can only be applied in

translucent media in extremely thin samples, typically ranging from 1 mm to approximately 1.4 cm (Darnault *et al*. 1998; Corapcioglu and Fiedirchuck 1999; Jones and Smith 2005; O'Carroll and Sleep 2007 Bob *et al.* 2008). The most recent research conducted with transparent soils recommended using samples with a thickness of less than 5 cm (Ezzein and Bathurst 2010).

Tidwell and Glass (1994) and Schroth *et al.* (1998) derived deterministic equations from the study of light transmission through a sample, in order to quantify the presence of NAPLs in porous media by means of image analysis. From these initial approaches, Niemet and Selker (2001) demonstrated the physical meaning of the fit parameters, to relate the saturation of water with the GLs of each pixel as follows:

$$S_w = \left(1 - \frac{\ln\left\{I_n\left[\left(\tau_{sw}/\tau_{so}\right)^{2k} - 1\right] + 1\right\}}{2\varsigma \ln\left(\tau_{sw}/\tau_{so}\right)}\right)\left(1 - S_{wr}\right) + S_{wr} \tag{3}$$

where S_w is the water saturation, S_{wr} is the irreducible water saturation, ς is the number of pores that have to be trasversed by the light from the source to the camera, τ_{sw} y τ_{sNAPL} are the light transmission factors of the sand-water mixture and of the sand-NAPL mixture, respectively, and I_n is a normalized light intensity (equation 4).

$$I_n = \frac{I - I_d}{I_s - I_d} \tag{4}$$

where I_d and I_s are light intensities determined in completely dry samples and water saturated samples, respectively.

Schroth *et al*. (1998b) had no success in determining NAPL saturation using this model, given that the light refraction indices of NAPL and water were the same in their experiments. However, Glass *et al*. (2000) were able to successfully apply this method to quantify the amount of TCE doped with oil red within the pores of silica sand samples.

Recently, Bob *et al.* (2008) combined Beer's and Fresnel's laws for light transmission, absorption and diffraction, and derived the following equation to determine the NAPL saturation:

$$S_{NAPL} = \frac{\ln I_s - \ln I}{\ln I_s - \ln I_{NAPL}} \tag{5}$$

where I_{NAPL} and I are light intensities when the sample is completely saturated with NAPL, and when the sample simultaneously contains NAPL and water inside the pores. The main advantage of this method is that only light intensities are needed to compute S_{NAPL}, and no specific calibration is needed.

Light reflection methods require that the processes that occur at the visible face of the sample must be representative of the entire sample. These methods do not require translucent samples. Traditionally, there are no analytical analyses involved to determine the relation between the intensity of the reflected light and the properties of the sample, and therefore these relationships are commonly presented as empirical relationships. Most known equations linearly relate reflected light intensity and moisture content (Darnault *et al*. 1998a) and solute concentration (Huang *et al*. 2002; Barns *et al*. 2012). This method was also successfully employed to monitor the displacement of colloids (Bridge *et al*. 2006; Bridge *et al.* 2009). However, to the authors' knowledge, there have been no accurate attempts presented that relate the intensity of reflected light and the amount of immiscible fluid phases present in the porous media.

Oostrom *et al*. (2007) and Kamaruddin *et al*. (2011) presented a detailed review analyzing different approaches to conducting immiscible displacement tests including different imaging techniques. They concluded that these photographic methods have the advantage of instant acquisition time and the ability to monitor processes; however, the main disadvantages are related to the need for specific calibrations in order to obtain accurate results. In addition, no previous works have reported the analysis of soil properties by means of complementary images used to reconstruct three dimensional flow processes.

MATERIALS AND METHODS

Soils and fluids

In this research, four different soil samples were studied: coarse sand, fine sand, medium sand, and silty sand composed of silt (25%) and coarse sand (75%). Sand samples were obtained from the Anisacate river basin in Córdoba Province while silts were typical loess soils from the central part of Córdoba Province, obtained from two trenches excavated at the campus of the Universidad Nacional de Córdoba.

A qualitative optic diffraction test Showed that the sand was mainly composed of pure minerals including quartz (43%), feldspars (12%) and muscovite (1%) and rock fractions consisting of granite (38%) and other rocks in a smaller percentage. The silt mainly consisted of quartz, feldspar, volcanic glass and igneous rock fragments. The main grain size distribution properties of each soil are summarized in Table 1.

The fluids employed for the immiscible displacement tests were paraffin oil and water. The paraffin oil behaved as the displaced phase, while a solution of sodium fluorescein was used as the aqueous displacing fluid in all immiscible displacement tests. The paraffin oil had relative density ρ_{rel} = 0.846 (LNAPL), viscosity μ = 1.5 x 10^{-2} [Ns/m²], and was odorless, colorless, and non-soluble in water.

The sodium fluorescein solution was employed in order to improve the optical contrast between the fluid phases. Sodium fluorescein ($C_{20}H_{12}O_5$) is an organic molecule with a molecular weight equal to 332.306, which is completely miscible in water (CRC 2007).

Immiscible displacement tests

The tests were conducted in a fully transparent Plexiglas cell in order to monitor the immiscible displacement process. It was composed of top and bottom transparent plates, 25 mm thick, and a dividing wall. The sample in the cell had an square section7 cm in wide and, 7 cm high and a length of 14 cm. At each end of the sample, the cell has a triangular area, 3.5 cm in length, to place porous material coarser than the sample, in order to homogenize the flow into the sample. All parts of the cell were manufactured in plexiglass. A rubber membrane was positioned in between the contact of the plate and the dividing wall, in order to prevent fluid leakage and to guarantee the sealing of the cell. Stainless steel screws were used to secure the cell. Figure 1a shows the details of the experimental set up, and Figure 1b shows a plane view and the dimensions of the cell.

Most of tests were conducted in 7 cm-thick samples; however, to explore the effect of the thickness of the samples, one sample was tested using a dividing wall of 2.5 cm. As stated in the previous section, these sizes of samples are thicker than those commonly employed for light transmission techniques.

The testing procedure was as follows. First, the cell was filled with a mixture of oven-dried soil sample mixed with 10% by weight of paraffin oil. The cell was filled with the wet soil, with the aid of a blunt-tipped bar, 10.95 mm in diameter. Once the cell was closed, the inlet and outlet ports were connected to paraffin oil reservoirs with different total head pressures, and then paraffin oil was allowed to flow from bottom to top, injecting a fluid volume equal to twice the pore volume of the sample. Table 2 presents the main characteristics of all the specimens, including porosity, pore volume and hydraulic conductivity determined with the paraffin oil. The saturation procedure was the same as that applied in Montoro and Francisca (2011). The degree of saturation obtained in all the samples was well above 0.96.

A constant head tank containing the displacing fluid was then connected to the bottom port, while the upper side port was open and free to drain into a volumetric graduated flask (Figure 1a). This flask allowed direct volumetric measurement of the displacing and displaced fluid phases collected at different stages during the immiscible displacement tests. This evaluation was performed at different net pore volumes of flow (NPV) which is defined as the ratio between the volume of effluent and the volume of the voids of the specimen under test. Note that the specimens remain saturated (S_w+S_{po}=1) during the immiscible displacement test.

The cell was mounted in a dark room and its face was illuminated by means of two UV-light sources, positioned outside the cell, in front of it and to each side of the cell (Figure 1). Each lighting device had a power of 40 W and a working frequency of 50 Hz. Light was allowed to illuminate only the front face of the cell.

A high resolution digital picture of the illuminated face of the transparent cell was acquired after every NPV. The images were acquired by a Canon™ PowerShot A590 IS digital camera. This camera has the possibility to of manually adjusting its settings to acquire the pictures with optimal characteristics. The distance between the front face of the cell and the focal point of the camera lens was 70 cm.

At the end of each test, the cell was disassembled, and then the specimen was carefully sliced every two centimeters along its longitudinal axis, with the aid of a stainless steel spatula. The procedure employed is invasive, but extreme care was taken to alter the pore structure of the sample as little as possible. The spatula was carefully cleaned before each slicing in order not to incorporate foreign material in the sample. There were no visual indications of significant

volume or shape change after the slicing procedure or evidence of significant fluid redistribution. A digital image was taken of the cross-section of each slice and this was considered representative of the situation of the entire slice. For the processing procedure, the first 2 mm of each side of the sections were not considered, in order to reduce the impact of border effects because these were the part of the sample that could be significantly altered during the segmentation process.

Digital image analysis and calibration

Pictures captured to monitor the displacement of paraffin oil by the fluorescein solution were analyzed using the MATLAB image analysis toolkit. Color pictures were initially transformed into 8-bit gray scale images. The pictures were then geometrically corrected in order to ensure that each pixel of a sequence of images corresponded to a given position. To eliminate any possible environmental effects, a black window was placed at the left of the cell in order to have a known GL at that position in all pictures.

The GL of each pixel depends on the environmental conditions related to light distribution and camera settings, and also depends on the soil type and the relative amount of each fluid phase in the sample (Werth *et al.* 2010). Several exposure times and fluorescein concentrations were tested in order to find the one that optimized the exposure time and the fluid phase contrast. Figure 2 shows the change in the GL obtained for 5 different fluorescein concentrations in water and various exposure times. Optimal test conditions were obtained with an exposure time of 3.2 sec and a fluorescein concentration of 3%. Thereafter, light conditions and camera settings were kept constant and calibration curves relating the GL and water and paraffin oil content were prepared for each soil sample tested. A fluorescein concentration of 3% (vol/vol) does not produce significant changes in the physical properties of water (Ghanem *et al.* 2003).

Calibration curves relating the mean GL and the paraffin oil saturation were developed for each soil sample tested. This relationship can be represented with a linear function such as an equation (6). Table 3 summarizes the equation coefficients (6) and the degree of correlation for each soil sample tested.

$$S_{po} = mGL + n \tag{6}$$

All pictures were filtered using a mean Gaussian filter, sized 3 pixel x 3 pixel. The filter size was selected by considering the mean grain sizes, and pore and pixel sizes. Each pixel had a size of 0.17 mm and the mean particle diameters of the specimens were between 0.41 mm and 1 mm (Table 1). For that reason, pictures permitted the identification of individual grains, but isolated pores could not be identified given that pore sizes are usually approximately one order of magnitude less than grain sizes (Fetter 1993). Thus, each pixel averages the information of many pores. Table 1 also shows the number of grains with the mean particle size obtained that can be found in one pixel, the mean pore diameter obtained as D_p=0.077D_{50} (Fetter 1993) and the expected number of pores in each pixel. The sample porosity was considered to compute the expected mean number of grains or pores that can be found in each pixel.

Different GL histograms of the images acquired were obtained for each soil sample containing different amounts of paraffin oil (Figure 3). Results showed that the higher the paraffin oil content, the lower the mean GL and variance of histograms. The increase in mean GL is related to a larger average number of fluorescein molecules per pixel. The GLs decreased as the amount of fine particles (<74μm) increased (Table 3), which is explained because this sample is the one with less porosity (Table 2), which means that for each pixel there will be fewer sodium fluorescein molecules due to the greater presence of solid grains.

The degree of saturation degree of paraffin oil (S_{po}) was obtained by dividing the volumetric content of oil determined from the calibration models presented in Table 3 by the porosity of the soil sample. The degree of saturation with respect to water was computed as S_w=1-S_{po} given that there was no air inside the pores.

The saturation of paraffin oil, S_{po}, was computed for each pixel in three different ways. As a first approach, a Niemet and Selker (2001) type equation was applied, regarding the lighting conditions and employing the number of pores affected by the light as a fit parameter. The second approach consisted in applying a Bob *et al*. (2008) type equation. The last alternative consisted in applying the correlations presented in Table 3.

Then, the processed images were binarized in order to identify areas of the sample with occluded paraffin oil. The binarization of pictures was conducted using the image analysis software Image J. Every pixel with a *GL* higher than the mean *GL* obtained for the sample soil completely saturated with paraffin oil was supposed to be partially invaded by colored water.

This analysis enabled the distribution of ganglion sizes to be determined. A statistical description of the ganglion sizes was performed by means of the coefficient of curvature (C_c) and the coefficient of uniformity (C_u) of the ganglion size distribution curves:

$$C_c = \frac{d_{60}}{d_{10}} \tag{7}$$

$$C_u = \frac{d_{30}^2}{d_{60} d_{10}} \tag{8}$$

where d_{60}, d_{30} and d_{10} are ganglion diameters corresponding to 60%, 30% and 10% smaller, respectively.

RESULTS AND ANALYSIS

Immiscible displacement tests were monitored by means of digital image analysis and volumetric measurement. The saturation of paraffin oil in each sample decreased with the NPV during immiscible displacement tests. Figure 4 shows the change in NAPL saturation with the increase of the NPV's, and a saturation map at the final stage for each type of sample is included in the Figure. It is clear that, in terms of the final value reached by direct volumetric measurement, the mean saturation obtained in the image is higher because the picture does not consider the process in all the bulk of the sample. In all cases, computed saturations from equation (3) (Niemet and Selker 2001), equation (5) (Bob *et al.* 2008) and the equations proposed in this article (equation 6) failed to reproduce the direct volumetric measurements. Bob *et al.*'s method failed because it was developed from experiments conducted in translucent samples, which therefore consider the flow process averaged through all the thickness of the sample. The method proposed by Niemet and Selker (2001) provided the best approach to experimental data given that the parameter ς in equation (3) was used as a fit parameter of the measured data in this research. Finally, the equations developed in this research failed because they are based on the process that occurred in only one face of the sample, and thus do not necessarily reflect the effects that take place in the bulk of the sample.

The significant difference between the analysis computed from images and the paraffin oil saturations measured was produced by the dissimilar measurement volume of the methods used. The digital image analysis method made it possible to know the paraffin oil contents for each pixel at the visible face of the sample (local measurement), while the paraffin oil content of the entire sample can only be determined from the volumetric measurements, providing average values for the specimen under test.

Computed and measured S_{po} approached each other when the specimen thickness was reduced from 7.0 to 2.5 cm (Figure 5). This result confirmed that the relative significance of the immiscible displacement in the specimen body with respect to that observed at its surface increased with specimen thickness; however, for this small thickness it is not possible to acquire good quality pictures of different cross-sections of the samples at the end of the test, and so it is not possible to analyze the displacement in the bulk of the sample. Figure 5 also shows that both the Niemet and Selker (2001) and the Bob *et al*. (2008) models give good approximations at the beginning of the immiscible displacement, but they fail to produce accurate values of S_{NAPL} at high NPV's. In this case, the S_{NAPL} predicted with these two models resulted significantly higher than the measured values.

Although the Bob *et al.* (2008) method and this research method were not able to capture the immiscible displacement inside the specimen, these methods provided the unique opportunity of monitoring the advancing front and flow pattern during displacement and of identifying areas with trapped paraffin oil (Figure 6).

Figure 6 shows the NAPL saturation change due to the increase in NPV's for medium sand samples with almost the same porosity (refer to Table 2). specimens were tested under exactly the same conditions but disassembled at a NPV equal to 1, 5, 10, 15 and 20. This made it possible to evaluate the influence of time of permeation and micro heterogeneities on the emerging flow pattern. The effect of microheterogeneities on the flow pattern is not easily distinguished from the volumetric measurement curve since the results obtained for each sample are very similar.

Figure 6 shows three different NAPL saturation maps obtained from three specimens after 10 NPV's. At the same pore volume of flow, the emerging patterns in the visible face are quite different. Also the average saturation of NAPL differs from that computed from the image

analysis, which confirms that the spatial variability of pore sizes inside the specimen and pore scale heterogeneities control the immiscible displacement. For all the pictures in this study black pixels indicate the presence of paraffin oil while white pixels are used for water. Color scale was transformed into NAPL saturation using equation (6) and the parameters shown in Table 3, in order to easily quantify the NAPL presence in each part of the sample. However, all specimens showed that the paraffin oil saturation decreased with the increase of the NPV, and all of them tend to reach the same final NAPL saturation of approximately 0.15. These results highlight that the variability observed in the flow pattern occurring in different samples of the same materials at the same stage of the tests, is governed by the microheterogeneities of the porous media. This variability that occurs in the bulk of the sample is responsible for the different observed flow patterns, and in some cases the images captures only the process that takes place at the face of the sample and do not reflect the effects in all the volume of the soil.

The properties of the different particle sizes of the four soils tested influenced the final NAPL saturation obtained for each sample, as well as the displacement pattern during the replacement of paraffin oil by water inside the pores. Figure 7 shows the NAPL saturation maps obtained from digital image analysis of pictures acquired in samples of coarse sand. Final NAPL saturation tends to 0.05 for coarse sand, 0.22 for fine sand and 0.1 for silty sand. NAPL saturation maps of the final stage of these samples are included in Figure 4. Flow patterns obtained at different NPV's for the coarse and medium sand specimens changed significantly during the test, showing similar random behavior. As shown in Table 1, estimated pore sizes of fine and silty sand were smaller than for coarse and medium sand. Consequently, each pixel of the pictures taken for fine and silty sands summarizes the information of more pores than for the case of coarser sands. Under this condition, the possibility of having pores invaded simultaneously by water and paraffin oil in the same pixel increases when the mean particle size reduces. Flow velocities were sufficiently low, given that hydraulic gradients were equal to 1, and capillary forces prevailed with respect to viscous ones. Capillary forces gain relevance in porous media with smaller pore sizes, as stated in Young-Laplace´s equation (Dullien 1992). In those cases, when a NAPL is displaced by water (imbibition process), the smaller pores are first invaded by water, resulting in a more uniform liquid displacement (Lenormand *et al.* 1988).

Pictures of the cross-section taken at the end of each test enabled a pseudo-3D image of the displacing plume to be built for each sample. These images confirmed the importance of the 3D

nature of the immiscible displacement phenomenon. In many cases, the main advancing front took place almost in the central part of the specimen, as is shown in Figure 8. In all cases where the main displacement process occurred in the middle part of the sample, this could not be monitored during the test from pictures of the front face of the sample.

Pictures of each cross-section were also used to estimate the degree of saturation assuming that each-cross section is representative of a thickness equal to the distance between two consecutive sections. In this case, computed and measured saturations of paraffin oil show an excellent correlation between them (Figure 9). To the best of the authors' knowledge, there are no previously published results analyzing the displacement pattern in the bulk of the sample. These results allowed the presence of ganglia to be identified and the saturation of NAPL in porous media to be estimated locally, not only in the visible face but also inside the sample.

Paraffin oil ganglia were identified for the first time for natural soil samples, by analyzing the soil pictures. Pictures of each specimen taken at different NPV's were binarized, which allowed sectors with paraffin oil (black) to be isolated, completely surrounded by water (white). Figure 10a shows the paraffin oil ganglia size distribution obtained in a coarse sand sample for different NPV's. The ganglia size curves move toward the right when the NPV increases, indicating that ganglia sizes reduced during the displacement of paraffin oil by water. This reduction in ganglia size is justified by bubble collapse mechanisms and separation before displacement, since the NAPL employed is not soluble in water. These results enable ganglia size and ganglia size distribution changes during the immiscible displacement to be assessed, information which is of key importance for optimizing remediation techniques (Sharma and Reddy 2004) or for quantifying the effect of potential ganglia dissolution (Tick and Rincon 2009).

The evolution of ganglia size during immiscible displacement was captured with the coefficient of uniformity and curvature (Figure 10b). C_u is a measure of the uniformity of ganglion size distribution: as it tends closer to one, ganglion sizes tend to be the same and the distribution is extremely narrow. This is also reflected in the coefficient of curvature (C_c), which decreases as there are more ganglions with the same size or the distribution is narrower. C_c and C_u clearly showed smaller values at higher NPV's in the case of coarse sand, but this tendency was not so clear as the soil particles decreased, probably due to the influence of pixel size on averaging the information of multiple pores.

CONCLUSIONS

Image processing can be successfully employed to analyze immiscible displacement in natural porous media. The results obtained show that the saturation of paraffin oil in the specimen can be obtained from the gray level of pixels in digital image analysis. Different correlations were developed for this purpose for natural soil samples, confirming the trends reported in the literature for synthetic porous media. These equations present a high level of accuracy, with r^2 over 0.9 in most cases. However, the accuracy of predictions diminishes as the soil grain size decreases, given that each pixel may simultaneously capture information of pores saturated with paraffin oil and water.

The match between the saturations obtained from image analysis and those computed from direct volumetric measurement increases as the thickness of the sample decreases. In addition, good correlations can be obtained when the image analysis is extended to the cross-sections of the sample, since the images can capture the immiscible displacement that takes place inside the specimen.

The analysis shows that more uniform fluid displacements occur in samples with finer grains. The advancing front tends to be more uniform when the displacement takes place at a low hydraulic gradient, given the relative importance of capillary forces. In addition, pixels average the information of multiple pores when the pore size decreases.

The analysis proposed in this research allowed ganglia to be isolated and the evolution in size and distribution of areas with trapped paraffin oil during immiscible flow to be determined. Image analysis successfully captured that the size and number of ganglia tends to decrease during immiscible displacement, which can be numerically estimated by means of statistical parameters of the cumulative ganglion size distribution curves.

ACKNOWLEDGMENTS

This research was partially financed by the National Agency for the Promotion of Science and Technology (ANPCyT), CONICET and SECyT-UNC. M.A.M. thanks CONICET for the graduate fellowship during this research and F.M.F. thanks FCEFyN-UNC and ISEA-UNC for

their support. The views expressed in this manuscript reflect those of the authors and not of CONICET, ANPCyT, SECYT-UNC.

REFERENCES

Aggelopoulos, C.A. and Tsakiroglou, C.D., 2009. "A Multi-flowpath Model for the Interpretation of Immiscible Displacement Experiments in Heterogeneous Soil Columns". *Journal of Contaminant Hydrology*, 105(3-4):146-160.

Ahrenholz, B., Tolke, J., Lehmann, P., Peters, A., Kaestner, A., Krafczyk, M. and Durner, W., 2008. "Prediction of Capillary Hysteresis in a Porous Material Using Lattice – Boltzmann Methods and Comparison to Experimental Data and a Morphological Pore Network Model". *Advances in Water Resources*, 31(9):1253–1268.

Al-Raoush. R.I. and Willson, C.S., 2005. "Extraction of Physically Realistic Pore – Network Properties From Three Dimensional Synchrotron X-ray Microtomography Images of Unconsolidated Porous Media". *Journal of Hydrology*, 300(1-4):44–64.

ASTM, 2007. *Annual book of ASTM Standards*. Vol. 04.08. ASTM International. West Conshohocken, P.A.

Babadagli, T., 2007. "Development of Mature Oil Fields – A Review". *Journal of Petroleum Science and Engineering*, 57(3-4):221-246.

Barns, G.L., Wilson, R.D. and Thornton, S.F., 2012. "Fluorescent Dye Imaging of the Volume Sampled by Single Well Forced-Gradient Tracer Test Evaluated in a Laboratory Scale Aquifer Physical Model". *Journal of Contaminant Hydrology,* 128(1-4):58-70.

Blunt, M.J., 2001. "Flow in Porous Media – Pore – Network Models and Multiphase Flow". *Current Opinion in Colloid and Interphase Science*, 6(3):197–207.

Bob, M.M., Brooks, M.C., Mravik, S.C. and Wood, A.L., 2008. "A Modified Light Transmission Visualization Method for DNAPL Saturation Measurements in 2D Models". *Advances in Water Resources*, 31(5): 727–742.

Bridge, J.W., Banwart, S.A. and Heathwaite, A.L., 2006. "Non-Invasive Quantitative Measurement of Colloid Transport in Mesoscale Porous Media Using Time Lapse Fluorescence Imaging". *Environmental Sience and Technology*, 40(19):5930-5936.

Bridge, J.W., Heathwaite, A.L. and Banwart, S.A., 2009. "Measurement of Colloid Mobilization and Redeposition During Drainage in Quartz Sand". *Environmental Sience and Technology*, 43(15):5769-5775.

Chen, Z., Huan, G. and Ma, Y., 2006. *Computational Methods for Multiphase Flow in Porous Media.* SIAM. Philadelphia.

CRC, 2007. *Handbook of Chemistry and Physics* in: David R. Lide (Ed). 88th Edition. Boca Ratón.

Darnault, C.J.G., Throop, J.A., Di Carlo, D.A., Rimmer, A., Steenhuis, T.S. and Parlange, J.Y., 1998. "Visualization by Light Transmission of Oil and Water Contents in Transient Two – Phase Flow Fields". *Journal of Contaminant Hydrology*, 31(3-4):337–348.

Dillard, L.A. and Blunt, M.J., 2000. "Development of a Pore Network Simulation Model to Study Nonaqueous Phase Liquid Dissolution". *Water Resources Research*, 36(2):439-54.

Donaldson, E.C., Chilingarian, G.V. and Yen, T.F., 1985. *Enhanced Oil Recovery, I: Fundamentals and Analyses*. Elsevier, New York.

Dong, W. and Selvadurai, A., 2006. "Image Processing Technique for Determining the Concentration of a Chemical in a Fluid-Saturated Porous Medium". *Geotechnical Testing Journal*, 29(5):385–391.

Dullien, F.A.L., 1992. *Porous Media: Fluid Transport and Porous Structure*, 2nd Ed. Academic Press, San Diego.

Ezzein, F.M. and Bathurst, R.J. (2011). "A Transparent Sand for Geotechnical Laboratory Modeling". Geotechnical Testing Journal, 34(6): 1 – 12.

Fetter, C.W., 1993. *Contaminant Hydrogeology*, 2nd Ed, Prentice Hall, Upper Saddle River.

Francisca, F.M. and Arduino, P., 2007. "Immiscible Displacement Model for Anisotropic and Correlated Porous Media". *International Journal of Geomechanics*, 7(4):11–17.

Ghanem, A., Soerenz, T.S., Adel, M.M. and Thoma, G.J., 2003. "Investigation of Fluorescent Dyes as Partitioning Tracers for Subsurface Nonaqueous Phase Liquid (NAPL) Characterization". *Journal of Environmental Engineering*, 129(8):740–744.

Glass, R.J., Conrad, S.H. and Peplinski, W., 2000. "Gravity-Destabilizing Nonwetting Phase Invasion in Macroheterogeneous Porous Media: Experimental Observations of Invasion Dynamics and Scale Analysis". *Water Resources Research*, 36(11):3121-3137

Goldstein, L., Prasher, S.O. and Ghoshal, S., 2007. "Three – Dimensional Visualization and Quantification of Non-Aqueous Phase Liquid Volume in Natural Porous Media using a Medical X-Ray Computed Tomography Scanner". *Journal of Contaminant Hydrology*, 93(1-4):96-110.

Hassanizadeh, S.M. and Gray, W.G., 1993. "Toward an improved description of the physics of two–phase flow". *Advances in Water Resources*, 16(1):53–67.

Huang, W.E., Smith, C.C., Lerner, D.N., Thornton, S.F. and Oram, A., 2002. "Physical Modelling of Solute Transport in Porous Media: Evaluation of an Imaging Technique Using UV Exited Fluorescent Dye". *Water Research*, 36(7):1843-1853.

Iskander, M.G., Liu, J. and Sadek, S. 2002. "Transparent Amorphous Silica to Model Clay". *Geotechnical and Geoenvironmetal Journal*, 128(3): 262 – 273.

Jia, C., Shing, K. and Yortsos, Y.C., 1999. "Visualization and Simulation of Non–Aqueous Phase Liquids Solubilization in Pore Networks". *Journal of Contaminant Hydrology*, 35(4):363–387.

Kamaruddin, S.A., Sulaiman, W.N.A., Rahman, N.A., Zakaria, M.P., Mustaffar, M. and Sa'ari, R., 2011. "A Review of Laboratory and Numerical Simulations of Hydrocarbon Migration in Subsurface Environments". *Journal of Environmental Science and Technology*, 4(3):191-214.

Karaman, T. and Demiral, B.M.R., 2004. "Determination of Two and Three Phase Relative Permeability Values by Using a Pore Network Model". *Energy Sources*, 26:685–696.

Lenormand, R., Toubol, E. and Zarcone, C., 1988. "Numerical Models and Experiments on Immiscible Displacement in Porous Media". *Journal of Fluid Mechanics*, 189:165–187.

Lo, H., Kazunori, T., Iskander, M. and Yoon, S., 2010. "A Transparent Water – Based Polymer for Simulating Multiphase Flow". *Geotechnical Testing Journal,* 33(1): 1 – 13.

Mercer, J.W. and Cohen, R.M., 1990. "A Review of Immiscible Fluids in the Subsurface: Properties, Models, Characterization and Remediation". *Journal of Contaminant Hydrology*, 6(2):319–46.

Montoro, M.A. and Francisca, F.M., 2010. "Soil Permeability Controlled by Particle-Fluid Interaction". *Geotechnical and Geological Engineering*, 28(6): 851-864.

Montoro, M.A. and Francisca, F. M., 2011. "Permeabilidad Intrínseca de Suelos Arenosos con Presencia de Partículas de Limo y Arcillas". *Revista Internacional de Desastres Naturales, Accidentes e Infraestructura Civil*, 11(1): 16 – 30.

Newell, C.J., Acree, S.D., Ross, R.R. and Huling, S.G., 1995. *Light Nonaqueous Phase Liquids*. EPA Ground Water Issue, EPA/540/S-95/500.

Niemet, M.R. and Selker, J.S., 2001. "A New method for Quantification of Liquid Saturation in 2D Translucent Porous Media System Using Light Transmission". *Advances in Water Resources*, 24(6): 651–666.

Oostrom, M., Dane, J.H. and Wietsma, T.W., 2007. "A Review of Multidimensional, Multifluid, Intermediate-Scale Experiments: Flow Behavior, Saturation Imaging, and Tracer Detection and Quantification". *Vadose Zone Journal*, 6(3):610-637.

Panfilov, M. and Panfilova, I., 2005. "Phenomenological Meniscus Model for Two–Phase Flows in Porous Media". *Transport in Porous Media*, 58(1-2):87–119.

Pennell, K.D., Pope, G.A. and Abriola, L.M., 1996. "Influence of Viscous and Buoyancy Forces on the Mobilization of Residual Tetrachloroethylene During Surfactant Flushing". *Environmental Science and Technology*, 30(4):1328–1335.

Peters, S.B., Siemens, G. and Take, W.A., 2011."Characterization of Transparent Soil for Unsaturated Applications". *Geotechnical Testing Journal*, 34(5): 1 – 12.

Rashidi, M., Perrung, L., Tompson, A.F.B. and Kulp, T.J., 1996. "Experimental Analysis of Pore-Scale Flow and Transport in Porous Media. *Advances in Water Resources*, 3:163–80.

Sahimi, M., 1993. "Flow Phenomena in Rocks: From Continuum Models to Fractals, Percolation, Cellular Automata, and Simulated Annealing. *Review of Modern Physics*, 65(4):1393-1537.

Schroth, M.H., Istok, J.D., Selker, J.S., Oostrom, M. and White, M.D., 1998a. "Multifluid Flow in Bedded Porous Media; Laboratory Experiments and Numerical Simulations". *Advances in Water Resources*, 22(2):169–83.

Schroth M.H., Istok, J.D. and Selker, J.S., 1998b. "Three-Phase Immiscible Fluid Movement in the Vicinity of Textural Interfaces". *Journal of Contaminant Hydrology*, 32(1-2):1-23.

Sharma, H.D. and Reddy, K.R., 2004. *Geoenvironmental Engineering*. John Wiley and Sons. New Jersey.

Silin, D., Tomutsa, L., Benson, S.M. and Patzek, T.W., 2011. "Microtomography and Pore-Scale Modeling of Two Phase Fluid Distribution". *Transport in Porous Media*, 86(2):495-515.

Smith, J.E. and Zang, Z.F., 2001. "Determining Effective Interfacial Tension and Predicting Fingering Spacing for DNAPL Penetration Into Water Saturated Porous Media". *Journal of Contaminant Hydrology*, 48(1-2):167-183.

Suthersan, S.S., 1997. *Remediation Engineering, Design Concepts*. CRC. Press. Boca Raton, Florida.

Tick, G.R. and Rincon, E.A., 2009. "Effect of Enhanced Solubilization Agents on Dissolutions and Mass Flux from Uniformly Distributed Immiscible Liquid Trichloroethene (TCE) in Homogeneous Porous Media". *Water, Air and Soil Pollution*, 204(1-4):315-322

Tidwell, V.C. and Glass, R.J., 1994. "X-ray and Visible Light Transmission for Laboratory Measurement of Two-Dimensional Saturation Fields in Thin-Slab Systems. *Water Resources Research*, 30(11): 2873–2882.

Tsakiroglou, C.D., Theodoropoulou, M., Karoutsos, V., Papanicolau, D. and Sygouni, V., 2003. "Experimental Study of the Immiscible Displacement of Shear Thinning Fluids in Pore Networks". *Journal of Colloid and Interface Science*, 267(1):217–232.

van Duijn, C.J., Eichel, H., Helmig, R. and Pop, I.S., 2007. "Effective Equations for Two – Phase Flow in Porous Media: The Effect of Trapping on the Microscale". *Transport in Porous Media*, 9(3): 411 – 428.

Werth, C.J., Zang, C., Brusseau, M.L., Oostrom, M. and Bauman, T., 2010. "A Review of Non-Invasive Imaging Methods and Applications in Contaminant Hydrogeology Research". *Journal of Contaminant Hydrology*, 113(1):1-24.

Wildenschild, D., Hopmans, J.W., Rivers, M.L. and Kent, A.J.R., 2005. "Quantitative Analysis of Flow Processes in Sand Using a Synchrotron – Based X – Ray Microtomography". *Vadose Zone Journal*, 4:112-126.

Zang, Z.F. and Smith, J.E., 2001. “The Velocity of DNAPL Fingering inWater Saturated Porous Media: Laboratory Experiments and Mobile-Immobile Zone Model. *Journal of Contaminant Hydrology*, 49(1-2):335-353.

Zhao, H., Ge, L. and Luna, R. 2010. “Low Viscosity Pore Fluid to Manufacture Transparent Soil”. *Geotechnical Testing Journal*, 33(6): 1 – 6.

Table 1: Grain size properties of tested soils.

	Coarse sand	Medium sand	Fine sand	Silty sand
Mean particle diameter [mm]	1	0.7	0.41	0.72
Effective particle diameter, D_{10}, [mm]	0.41	0.21	0.15	0.02
Percentage of particles smaller than 0.074 mm	1.28	1.83	2.07	16.3
Clay fraction [%]	0	0	0	5.22
Mean pore diameter [mm] (Fetter, 1993)	0.077	0.054	0.031	0.055
Number of grains per pixels	0.025	0.048	0.12	0.051
Number of pores per pixels	2.11	4.67	17.61	3.28

Table 2: Main properties of tested samples.

Sample	n	Poral volume [cm^3]	NPV before testing	k_{oil} [m/s] before immiscible displacement
Coarse Sand	0.34	330.6	2	$1.08x10^{-4}$
Medium Sand	0.37 (±0.01)	364.6 (±10.79)	2	$7.34x10^{-6}$ ($\pm 3.51x10^{-6}$)
Fine Sand	0.46	448.4	2	$9.2x10^{-6}$
Silty Sand	0.27	262.5	2	2.78×10^{-6}

Table 3: Relations between volumetric paraffin oil content and gray levels for the different soils.

Sample	**m**	**n**	r^2	
Coarse sand	-0.04483	0.9530	0.98	(T3.1)
Medium sand	-0.03964	0.8101	0.97	(T3.2)
Fine sand	-0.03744	0.6633	0.93	(T3.3)
Silty sand	-0.07218	0.7715	0.82	(T3.4)

FIGURE CAPTIONS

Fig. 1. (a) Setup for the immiscible displacement tests and image acquisition. **(b)** Plane view of the transparent plexiglass cell.

Fig. 2. Influence of fluorescein concentration and exposure time on gray level

Fig. 3. Gray levels distribution histograms for medium sand contaminated with different amounts of paraffin oil.

Fig. 4. Paraffin oil saturation change during immiscible displacement tests. (a) coarse sand, (b) medium sand, (c) fine sand, (d) silty sand.

Fig. 5. Paraffin oil saturation determined by digital image analysis and direct volumetric measurement in a 2.5 cm thick medium sand sample.

Fig. 6. NAPL saturation change with the number of pore volumes of flow in medium sand samples. Pictures show the NAPL saturation maps of three different medium sand sample at NPV = 10.

Fig. 7. NAPL saturation distribution on the front face of coarse sand at different stages of immiscible displacement tests. The arrow shows flow direction.

Fig. 8. Paraffin oil distribution in a medium sand sample after 1 Npv of flow. (a) Geometry of the sample, (b) NAPL distribution maps of different transversal sections of the samples.

Fig. 9. Comparison of the NAPL saturation determined at the end of different tests by digital image analysis of pictures of the front face of the sample and pictures from the transversal sections of the sample. 45º line represents perfect fitting.

Fig. 10. a) Ganglia sizes cumulative distribution curves for coarse sand; b) influence of Npv on the coefficient of curvature and coefficient of uniformity.

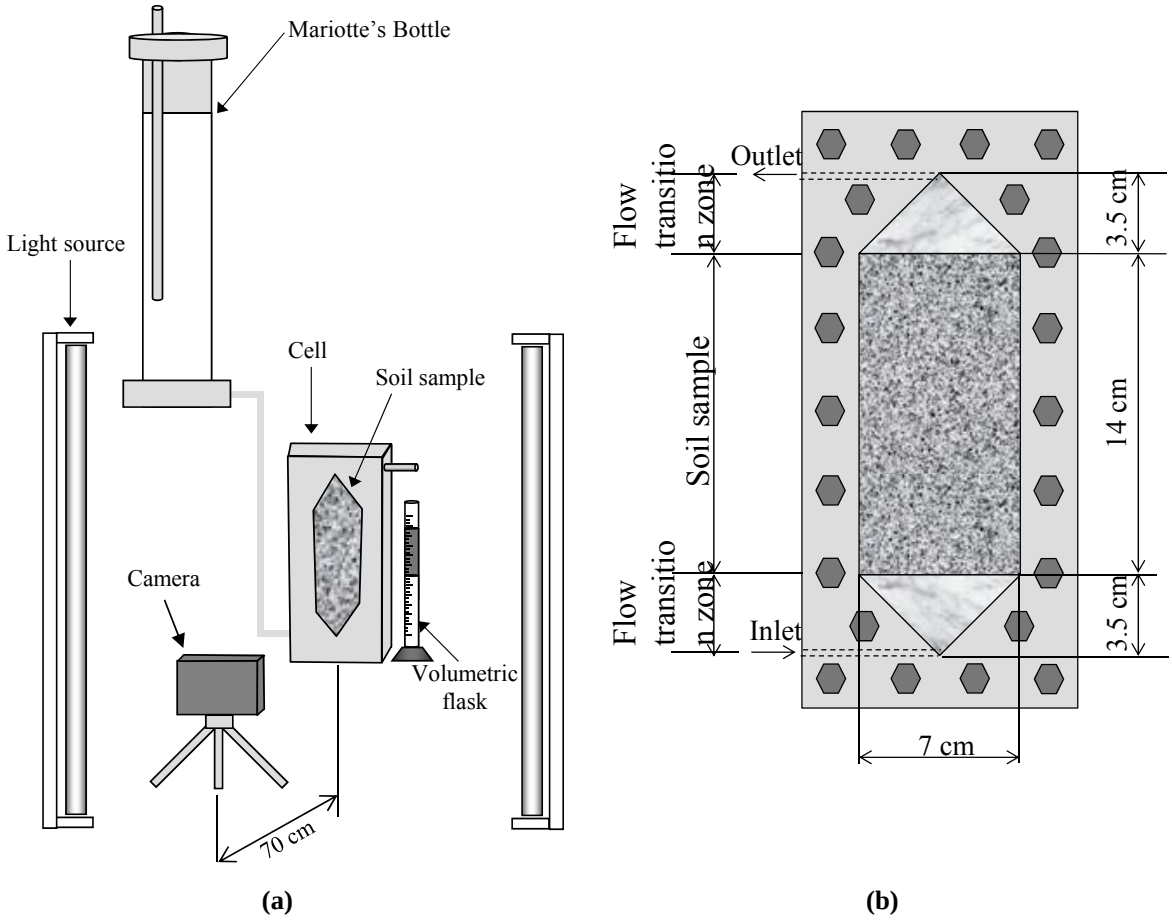

Fig. 1. (a) Setup for the immiscible displacement tests and image acquisition. **(b)** Plane view of the transparent plexiglass cell.

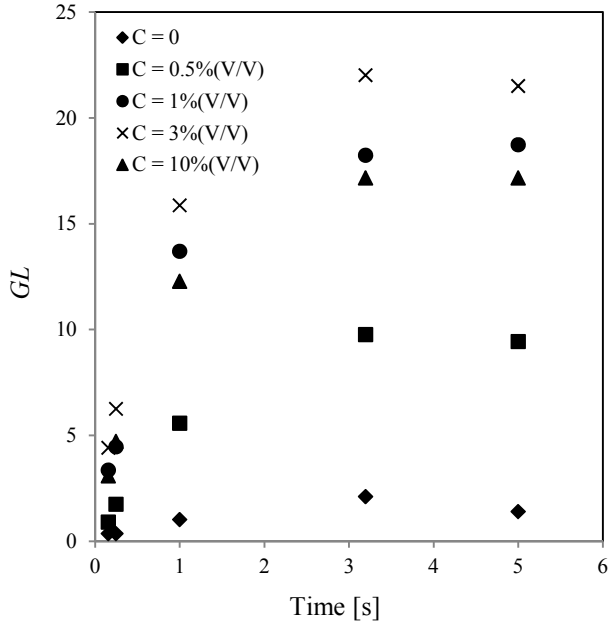

Fig. 2. Change in the gray level with the change of fluorescein concentration and exposure time.

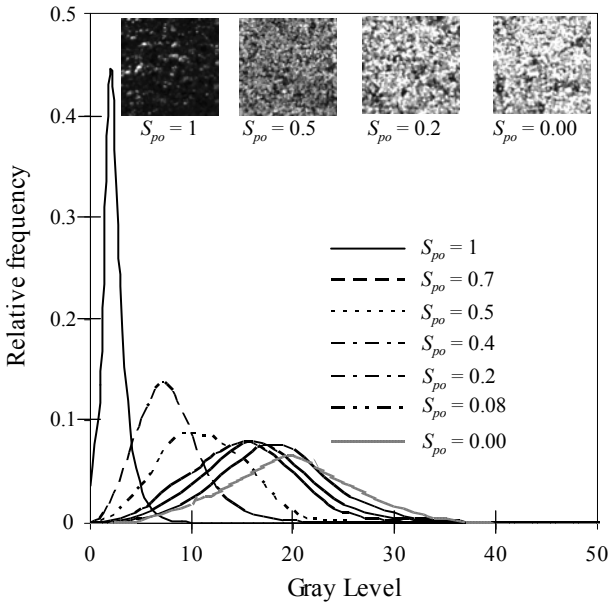

Fig. 3. Gray levels distribution histograms for medium sand contaminated with different amounts of paraffin oil. (Black: paraffin oil, whit: water).

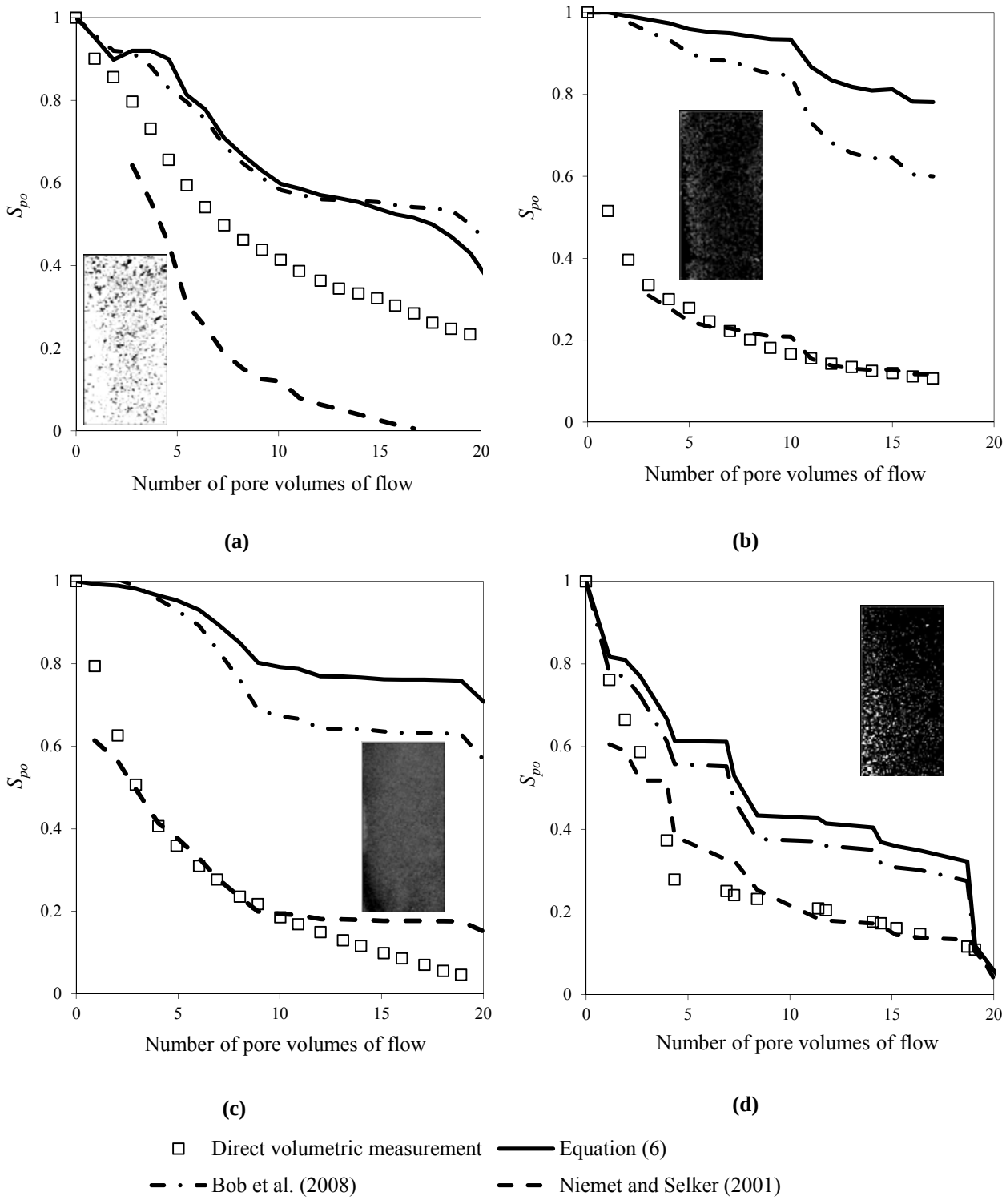

Fig. 4. Paraffin oil saturation change during immiscible displacement tests. (a) coarse sand, (b) medium sand, (c) fine sand, (d) silty sand. Images show local NAPL saturation at the visible face, black and white are S_{po}=1 and S_{po} =0, respectively.

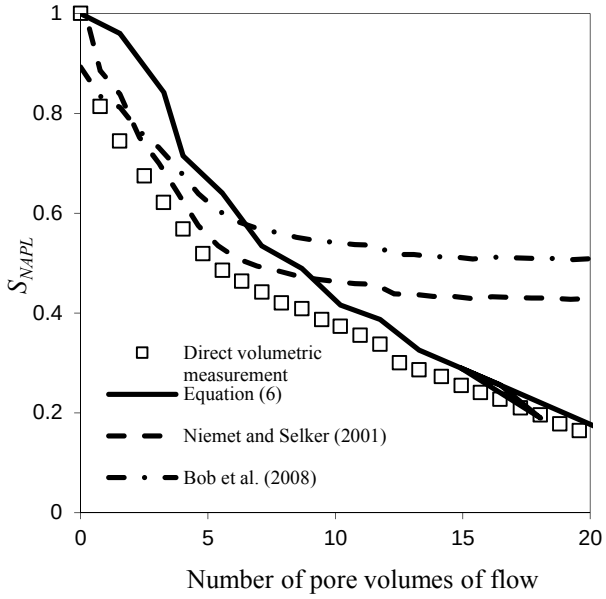

Fig. 5. Paraffin oil saturation determined by digital image analysis and direct volumetric measurement in a 2.5 cm thick medium sand sample.

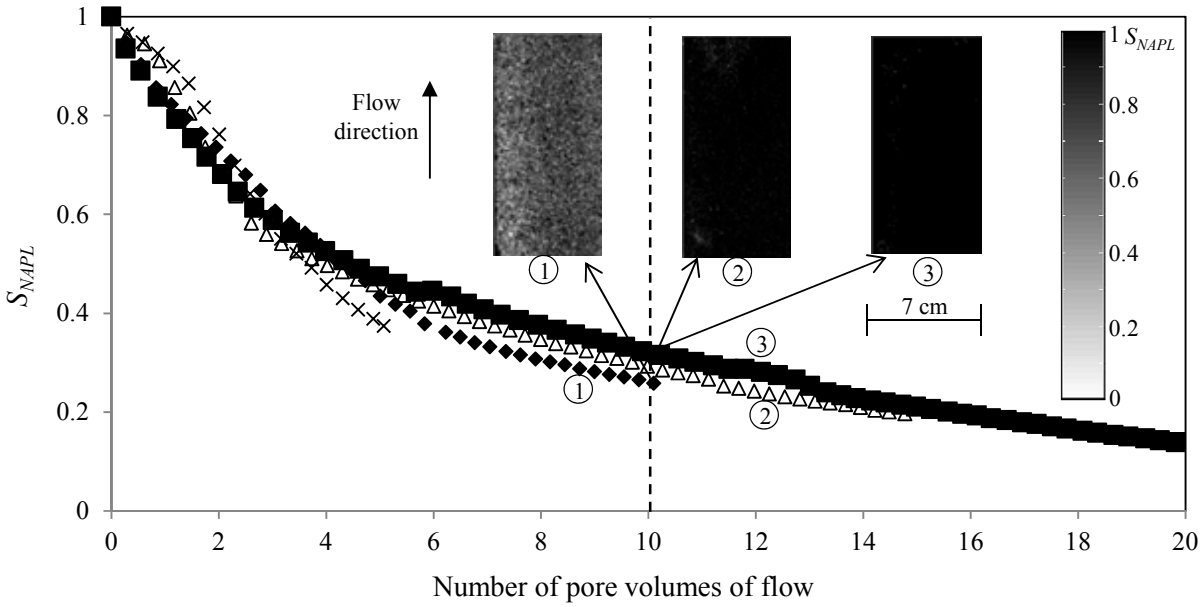

Fig. 6. NAPL saturation change with the number of pore volumes of flow in medium sand samples. Pictures show the NAPL saturation maps of three different medium sand sample at NPV = 10.

NPV = 0	1	5	10	15	20
$S_{NAPLavg}$ = 1	0.9	0.61	0.41	0.31	0.22

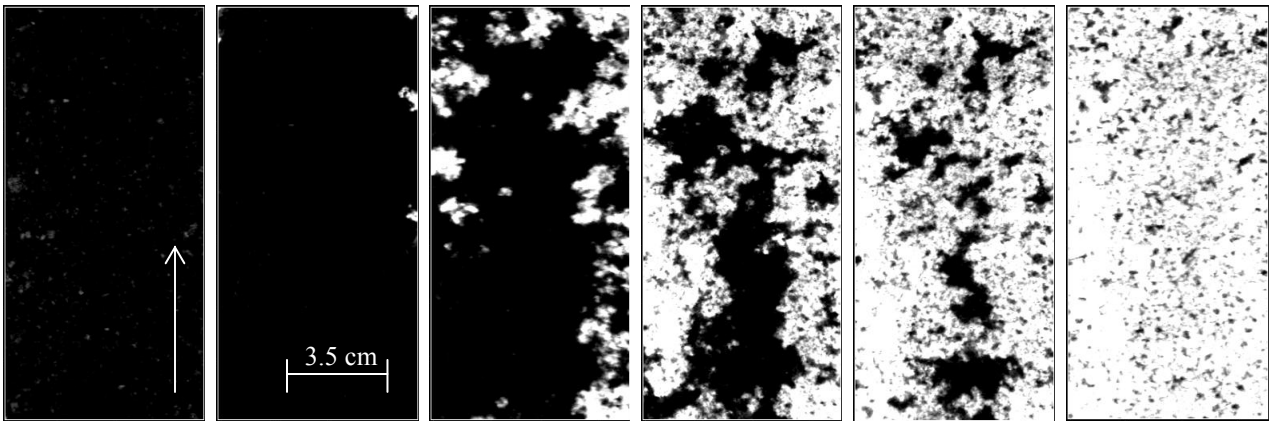

Fig. 7. NAPL saturation distribution on the front face of coarse sand at different stages of immiscible displacement tests. The arrow shows flow direction.

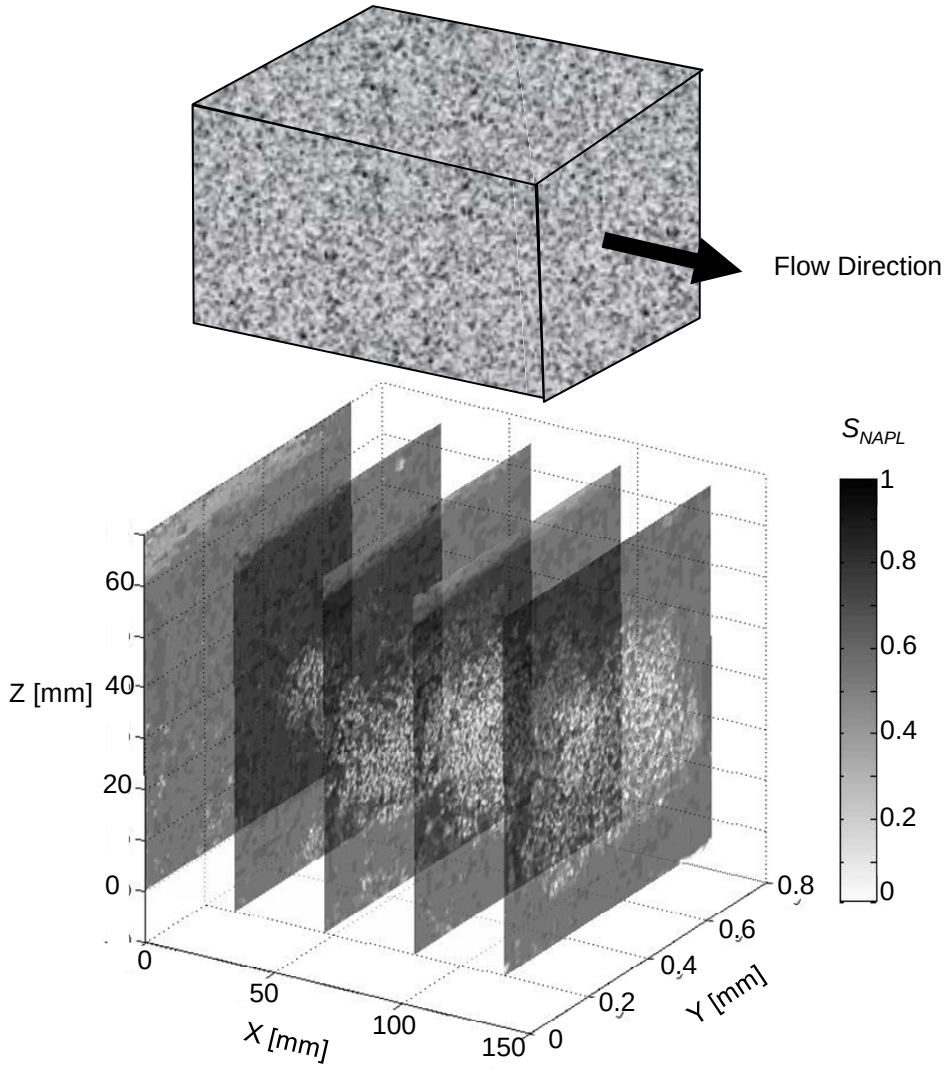

Fig. 8. Paraffin oil distribution in a medium sand sample after 1 Npv of flow. (a) Geometry of the sample, (b) NAPL distribution maps of different transversal sections of the samples.

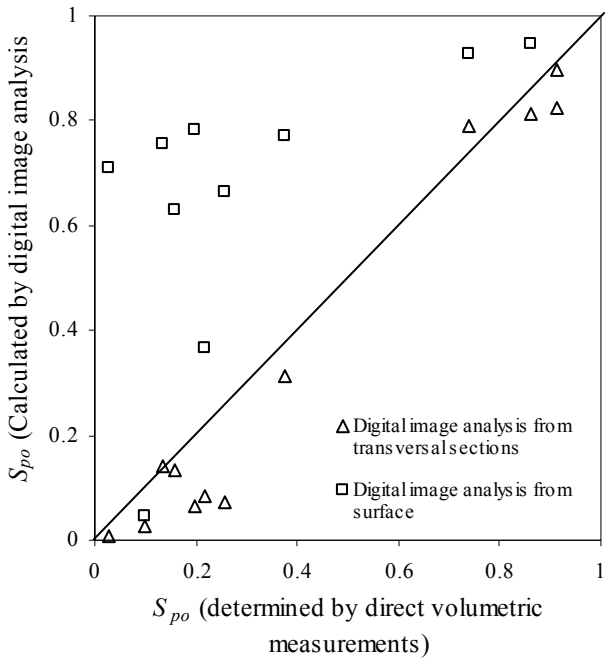

Fig. 9. Comparison of the NAPL saturation determined at the end of different tests by digital image analysis of pictures of the front face of the sample and pictures from the transversal sections of the sample. 45º line represents perfect fitting.

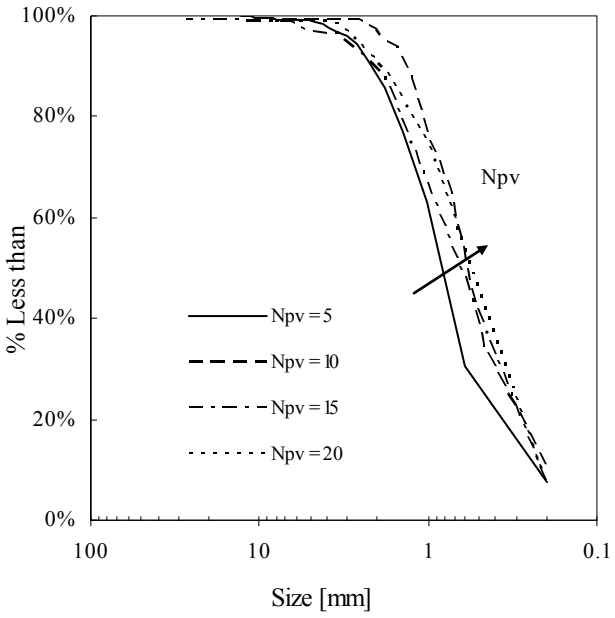

(a)

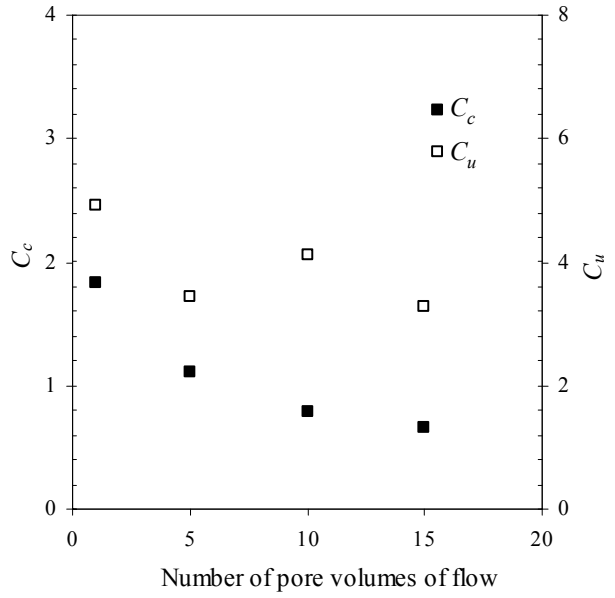

(b)

Fig. 10. a) Ganglia sizes cumulative distribution curves for coarse sand; b) influence of Npv on the coefficient of curvature and coefficient of uniformity.